PROCEEDINGS, 45th Workshop on Geothermal Reservoir Engineering
Stanford University, Stanford, California, February 10-12, 2020
SGP-TR-216

Viscoacoustic-Waveform Inversion with the Local Frequency Shift: Application to the Blue Mountain Geothermal Field

Zongcai Feng[1], Lianjie Huang[1], and Trenton Cladouhos[2]

[1]Los Alamos National Laboratory, Los Alamos, NM 87545, USA; [2]Cyrq Energy, Inc., 4010 Stone Way North, Seattle, WA 98103

zongcai@lanl.gov; ljh@lanl.gov; trenton.Cladouhos@cyrqenergy.com

Keywords: Attenuation, Blue Mountain, geothermal reservoir, local frequency shift, short-time Fourier transform

ABSTRACT

Accurate estimate of seismic attenuation is valuable for geothermal reservoir characterization. Seismic waves traveling through geothermal reservoirs result in amplitude loss and velocity dispersion. Waveform inversion has the potential to reconstruct subsurface attenuation distributions. However, a reliable estimate of an attenuation model is difficult because the amplitudes of seismic data are affected by other factors such as scattering or changes in impedance in addition to attenuation. We develop a novel viscoacoustic waveform inversion method for addressing the difficulties in attenuation inversion. To mitigate the effect of amplitude distortion, we analyze the local peak/centroid-frequency shifts using short-time Fourier transform, and then use the frequency shifts as a misfit function in the waveform inversion to invert for the attenuation model. We apply the method to 2D surface seismic data acquired at the Blue Mountain geothermal field, and our results show that the geothermal reservoir exhibits higher attenuation than the surrounding regions.

1. INTRODUCTION

The Blue Mountain geothermal field, located in northern Nevada, has been in operation since November 2009. The power plant was designed to generate 49.5 MW of gross capacity and 39.5MW of net capacity. From 2009 to 2013, the resource experienced significant temperature decline because of reinjection into wells on the west side of the field, down-dip of the production zone. Since 2013, all but one of the western injectors have been idle, with reinjection moved to the northern and northeastern edges of the field. Wells on the southern edge of the field, where new reinjection could mine significant stranded heat-in-place, remain idle because of low permeability. Former injection wells at the western edge of the field were initially very hot but they may not re-heat to pre-injection temperatures. Thus, new, hot production wells at the western edge of the field may be needed to bring the plant production back up to initial production.

An active seismic survey along seven 2D lines was carried out at the Blue Mountain geothermal field in 2007 for subsurface characterization (Optim, 2007). Optim built a tomography velocity model using refraction tomography for each line of seismic data. For better subsurface characterization, Huang et al., (2018) obtain high-resolution subsurface velocity model by using seismic anisotropic full waveform inversion (FWI) at the Blue Mountain geothermal field.

Beside velocity model, subsurface attenuation model is also valuable information for providing independent constraints on the rock/fluid properties of the reservoir target. When seismic waves propagate in the Earth, seismic waveforms suffer from amplitude decay and velocity dispersion caused by seismic attenuation. Though FWI holds the ability of obtaining both the subsurface velocity and attenuation properties (Virieux and Operto, 2009; Prieux et al., 2013) by minimizing the waveform difference between the observed and predicted data, a reliable estimate of an attenuation model is difficult because the amplitudes of seismic data are affected by other factors such as scattering or changes in impedance in addition to attenuation.

A more reliable approach than any FWI-like algorithm is to invert for an attenuation model that minimizes the differences between the peak frequencies of the observed and the predicted data and smeared the shifts along raypaths to update the attenuation model (Quan and Harris, 1997). The peak frequencies are obtained from the amplitude spectra of the traces. To handle complex wave propagation, the predicted data and the raypaths can be modeled using the viscoacoustic wave equation (Dutta and Schuster, 2016). However, current frequency-shift approach is limited to the transmission arrivals, where the amplitude spectra is calculated using the whole trace (Dutta and Schuster, 2016), or it requires picking of the key reflection events/reflectors before calculating the amplitude spectra (Chen et al., 2018).

We develop a novel viscoacoustic-waveform inversion method to invert for an attenuation model that minimizes the local peak-frequency difference between the observed and the predicted data. The local peak frequencies are obtained using short-time Fourier transform (STFT) of seismic traces. STFT estimates the amplitude spectra of one or a few local events within a local time window, thus not limited to transmission arrivals or picked reflection events. The residual trace for backprojection is obtained by weighting all local events in the trace with the corresponding local frequency shifts. The forward modeling and the backprojection of residuals are computed using finite-difference solutions to the time-domain viscoacoustic wave equation characterized by the standard linear solid (SLS) mechanism (Carcioneet al., 1988; Blanch et al., 1995).

We firstly demonstrate our new viscoacoustic-waveform inversion method using asynthetic example. We then apply our method to seismic data along Line 1, Line 2 and Line 7 acquired at the Blue Mountain geothermal field, and our results show that the geothermal reservoir exhibits higher attenuation than the surrounding regions.

2. METHODOLOTY

Our attenuation method attempts to invert for a Q model which minimize the misfit function

$$\varepsilon = \frac{1}{2}\sum_{s}\sum_{r}\sum_{n}\left(f_c^{pred}(\mathbf{x}_s,\mathbf{x}_r,t_n) - f_c^{obs}(\mathbf{x}_s,\mathbf{x}_r,t_n)\right)^2 = \frac{1}{2}\sum_{s}\sum_{r}\sum_{n}\Delta f_c^{\,2}, \tag{1}$$

where the summation in equation 1 is over all sources (s), receivers (r), and the local time windows (n) for STFT. Parameter f_c is the peak frequency of the amplitude spectra of local events (shown by the dash black curve in Figure 1). The peak frequency f_c experiences a downshift during the propagation in an attenuation media because the high-frequency components of the seismic signal are attenuated more rapidly than the low-frequency components (Quan and Harris, 1997).

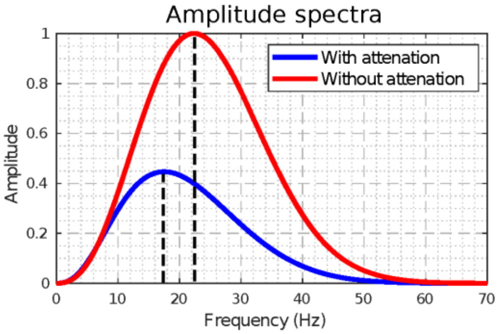

Figure 1: Comparison between the amplitude spectra of a single event travel through a medium with attenuation and without attenuation. The dash black curve indicates the peak frequency.

For real data case, the peak frequency for the arrivals is difficult be accurately estimated. In such cases, the peak frequency f_c can be approximated by the centroid-frequency shift of a trace as

$$f_c = \frac{\int_0^f f \times A(f)}{\int_0^f A(f)}, \tag{2}$$

where $A(f)$ is the amplitude for a frequency f.

3. METHODOLOTY

3.1 Synthetic Example

We first demonstrate the effectiveness of our viscoacoustic-waveform inversion method using a synthetic example. Figures 2a and 2b display the true velocity and density models, respectively. A smooth true Q model is shown in Figure 2c. We use the true velocity model as the initial velocity model, while the initial density and Q models are homogenous with 2080 kg/m^3 and 1/Q=0. Note that we only invert for the Q model.

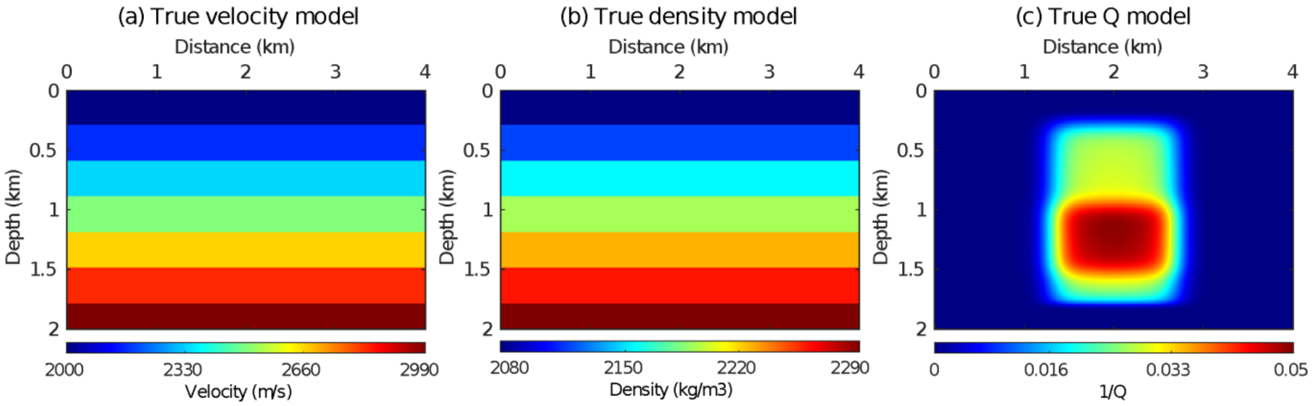

Figure 2: (a) True velocity model, (b) true density model and (c) true Q model.

Figures 3a, 3b and 3c show the Q models inverted by FWI, conventional frequency-shift method that computes the amplitude spectrum of a whole trace and our local frequency-shift method that computes the local the amplitude spectrum. It is evident that our local frequency-shift method successfully reconstructs the Q model while conventional frequency-shift method does not. We also demonstrate that FWI fails to the invert for an accurate Q model because of the changes in impedance between the true and initial model, while our method is immune to this amplitude problem.

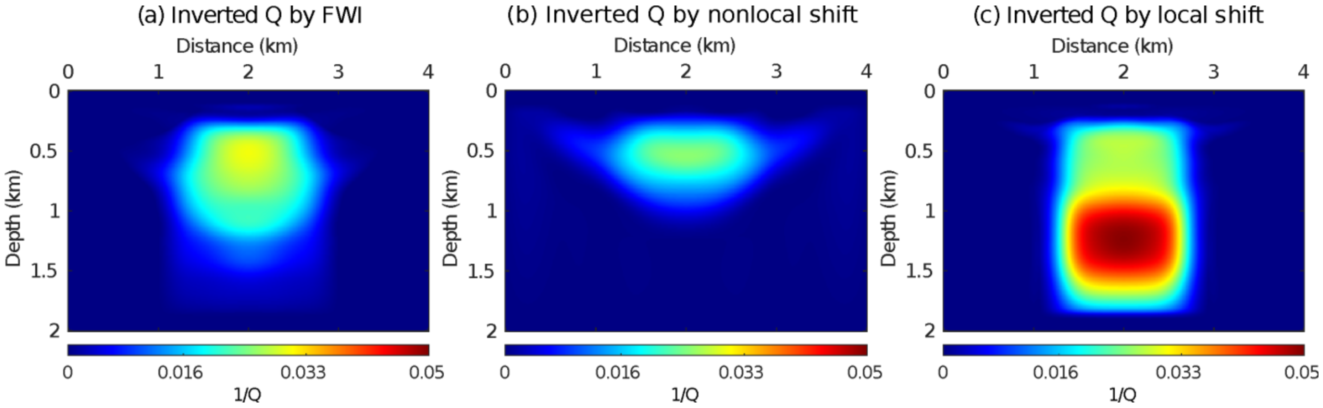

Figure 3: Inverted Q model by (a) FWI, (b) conventional frequency-shift method and (c) local frequency-shift method.

3.2 Field Data Example at Blue Mountain Geothermal Field

We apply our viscoacoustic-waveform inversion method to the surface seismic data acquired at the Blue Mountain geothermal field. Figure 4 shows the seismic acquisition survey conducted in 2007. We apply our new method to seismic data along Line 1, Line 2 and Line 7. The P-wave models used for our viscoacoustic-waveform inversion are the FWI models from Huang et al., (2018), as shown in Figure 5. The initial attenuation models are homogeneous. The inverted Q models using our method for Line 1, Line 2 and Line 7 are display in Figures 6a and 6b. The results show very strong attenuation anomalies ($Q \approx 20$) at the shallow surface and located at deeper area of the east side of the field.

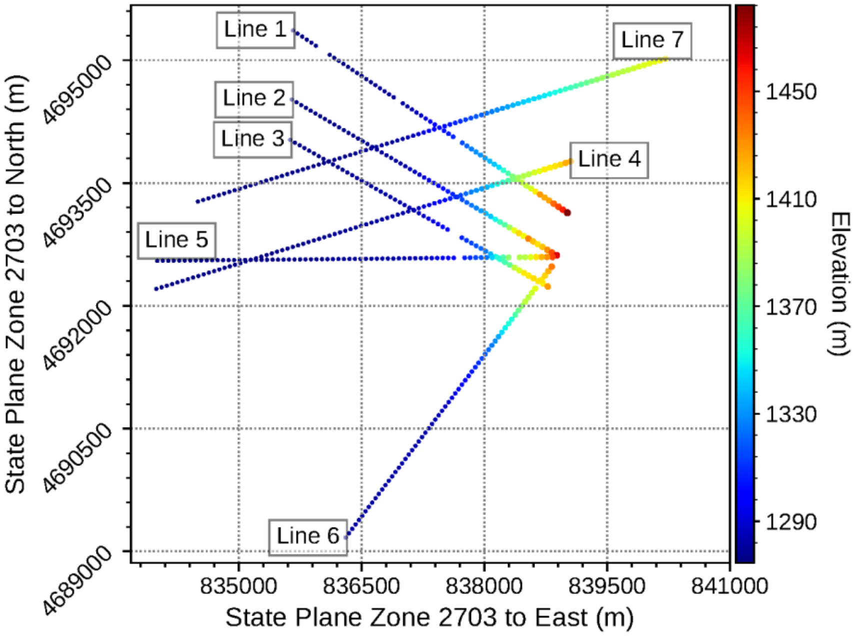

Figure 4: Seven 2D lines for acquiring active seismic data at the Blue Mountain geothermal field.

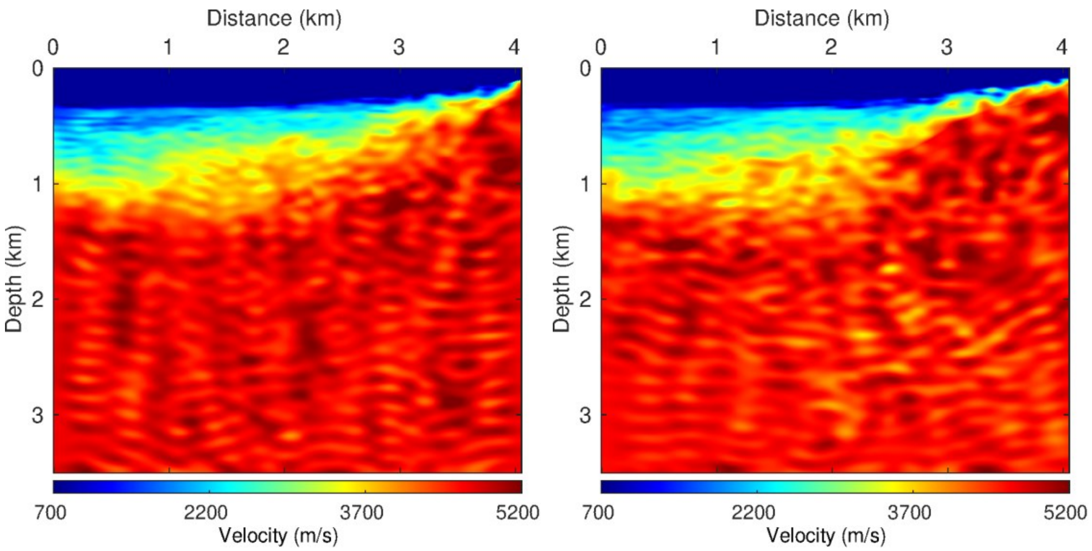

(a) Velocity model for Line 1

(b) Velocity model for Line 2

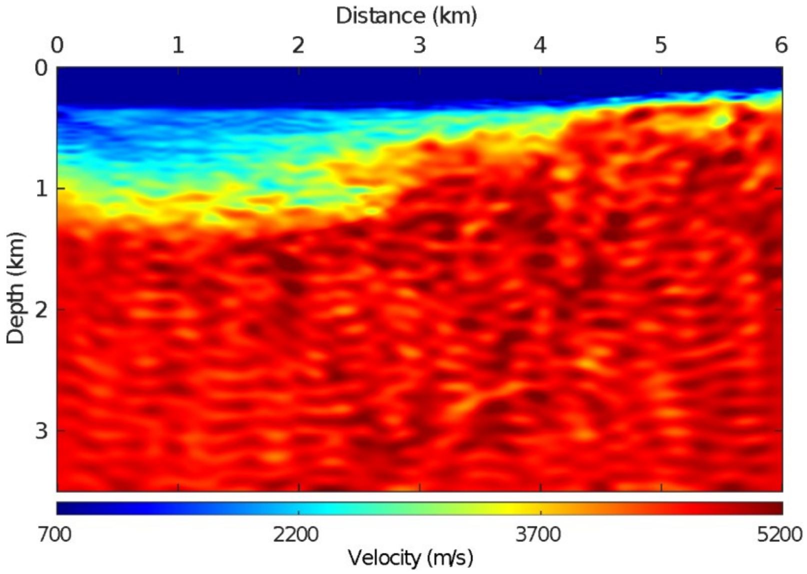

(c) Velocity model for Line 7

Figure 5: FWI velocity models for (a) Line 1, (b) Line 2 and (c) Line 7 (Huang et al., 2018).

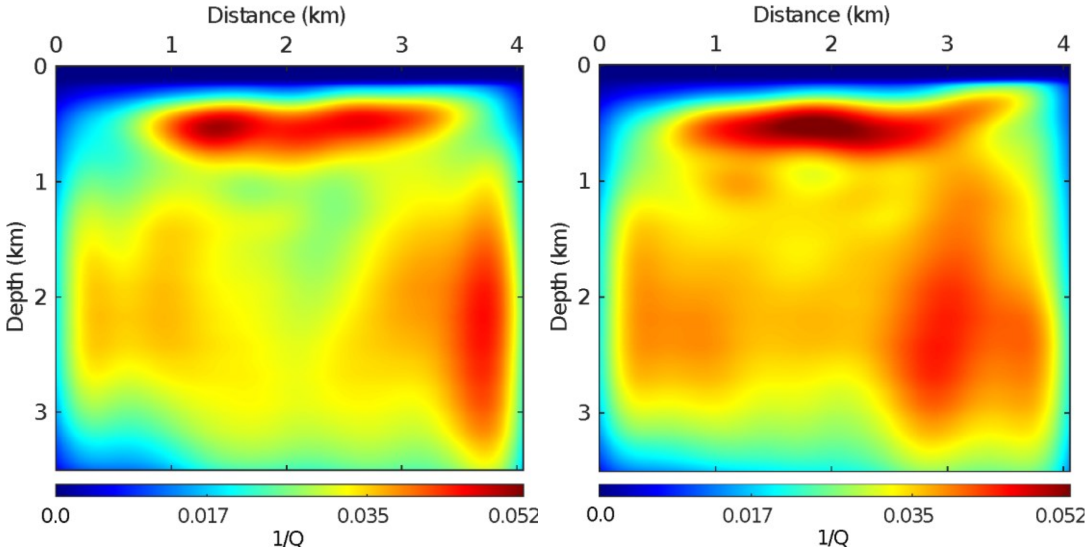

(a) Inverted Q model for Line 1

(b) Inverted Q model for Line 2

(c) Inverted Q model for Line 7

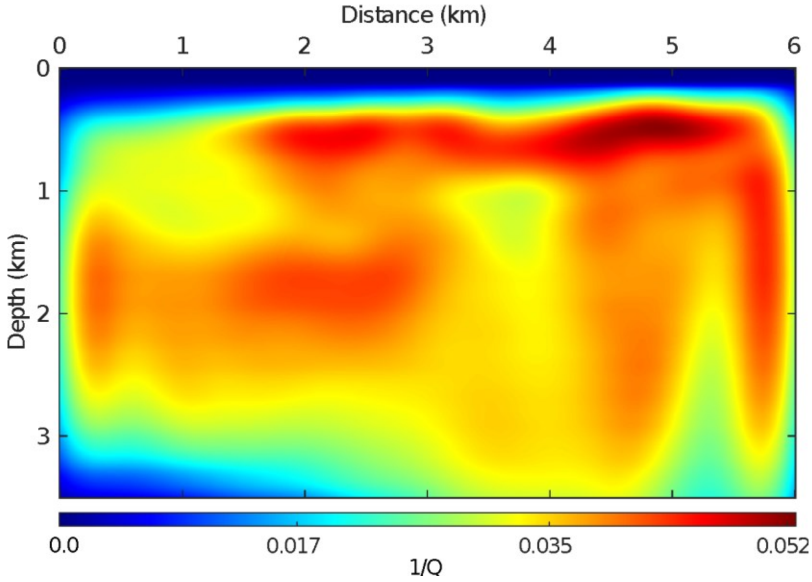

Figure 6: Inverted Q models by our viscoacoustic-waveform inversion for (a) Line 1, (b) Line 2 and (c) Line 7.

4 CONCLUSIONS

We have developed a novel viscoacoustic-waveform inversion method using the local peak/centroid frequency shifts between the observed and the predicted data. The local peak/centroid frequency is calculated using local amplitude spectrum with short-time FFT. The synthetic example demonstrate that our new method is more reliable than FWI because it is less prone to the amplitude errors in the data. We have applied our new method to three lines of surface seismic data acquired at the Blue Mountain geothermal field. Our results show very strong attenuation anomalies at the shallow region and located at deeper area of the east side of the geothermal field.

5 ACKNOWLEDGMENTS

This work was supported by the Geothermal Technologies Office (GTO) of the U.S. Department of Energy (DOE) through the Los Alamos National Laboratory (LANL), which is operated by Triad National Security, LLC, for the National Nuclear Security Administration (NNSA) of U.S. DOE under Contract No. 89233218CNA000001. This research used resources provided by the LANL Institutional Computing Program, which is supported by the U.S. DOE NNSA under Contract No. 89233218CNA000001.

REFERENCES

AltaRock Energy, Inc.: Blue Mountain Resource Review (2013).

Blanch, J. O., Robertsson, J. O., & Symes, W. W.: Modeling of a constant Q: Methodology and algorithm for an efficient and optimally inexpensive viscoelastic technique, *Geophysics*, **60(1)**, (1995) 176-184.

Carcione, J. M., Kosloff, D., and Kosloff, R.: Viscoacoustic wave propagation simulation in the earth, *Geophysics*, **53**, (1988), 769-777.

Chen, Y, Dutta, G., and Schuster, G. T.: Image-domain Q inversion, *SEG Technical Program Expanded Abstracts*, (2018) 4121-4125.

Dutta, G., and Schuster, G. T.: Wave-equation Q tomography, *Geophysics*, **81(6)**, (2016), R471-R484.

Prieux, V., Brossier, R., Operto, S., and Virieux, J.: Multiparameter full waveform inversion of multicomponent ocean-bottom-cable data from the Valhall field. Part 1: Imaging compressional wave speed, density and attenuation, *Geophysical Journal International*, **194(3)**, 1640-1664.

Quan, Y., & Harris, J. M.: Seismic attenuation tomography using the frequency shift method, *Geophysics*, **62(3)**, (1997), 895-905.

Swyer, M., Uddenberg, M., Nordin, Y., Cladouhos, T., and Petty, S.: Improved Injection Strategies at Blue Mountain, Nevada Through an Improved Conceptual Model, Tracer Testing, and Injection-production Correlation, *Proceedings*: 41st Workshop on Geothermal Reservoir Engineering, Stanford, CA (2016).

Virieux, J., and Operto, O.: An overview of full-waveform inversion in exploration geophysics, *Geophysics*, **74**, (2009), WCC1-WCC26.